www.czasopisma.pan.pl PAN POLSKA AKADEMIA NAUK www.journals.pan.pl

Arch. Metall. Mater. **63** (2018), 4, 2039-2049

DOI: 10.24425/amm.2018.125141

Z. BRYTAN*#

THE EROSION RESISTANCE AND MICROSTRUCTURE EVALUATION OF LASER SURFACE ALLOYED SINTERED STAINLESS STEELS

The sintered stainless steels of different microstructures (austenitic, ferritic and duplex) were laser surface alloyed with hard powders (SiC, Si_3N_4) and elemental alloying powders (Cr, FeCr, FeNi) to obtain a complex steel microstructure of improved properties. Laser surface alloying (LSA) involved different strategies of powder placing: the direct powder feeding to the molten metal pool and filling grooves machined on the sample surface by powder, and then laser surface melting. Obtained microstructures were characterised and summarised, basing on LOM, SEM and XRD analysis. The links between base material properties, like superficial hardness and microhardness, derived microstructures and erosion resistance was described. The LSA conditions and alloying powder placement strategies on erosion resistance was evaluated. The erosion wear is lower for Cr, FeCr, FeNi laser alloying, where powders were dissolved in the steel microstructure, and hard phases were not precipitated. Precipitations of hard phases (carbides, silicides, martensite formation) reduce erosion resistance of SiC alloyed stainless steel. The LSA with Si_3N_4 works better due to lack of precipitates and formation of a soft and ductile austenitic microstructure. The erosion wear at the impingement angle of 90° is high for hard and therefore brittle surface layers obtained as a result of alloying by hard particles (SiC, Si_3N_4). The softer and ductile austenitic stainless steel resist better than harder ferritic and duplex stainless steel material at studied erodent impingement angle.

Keywords: Sintered stainless steel, Duplex, Laser surface alloying, Erosion resistance

1. Introduction

Powder metallurgy (PM) stainless steel provides excellent advantages for traditional manufacturing routes, like milling for small size components of complex shape produced in large series, i.e. for automotive applications. Sintered stainless steels are cost effective and offer adequate corrosion resistance, oxidation resistance and mechanical strength. However, when compared to wrought stainless steels with the similar chemical composition the sintered materials show lower mechanical properties due to inherent porosity of traditional (uniaxial pressing, sintering) powder metallurgy components. The laser surface treatment (remelting, alloying, cladding, etc.) shows many possibilities to improve PM stainless steel properties, like the corrosion resistance, cavitation erosion resistance and wear resistance. Different strategies of laser surface treatment can be adopted for such improvement. One of the most promising is the laser surface alloying (LSA) with hard particles (carbides, nitrides, borides) or their compound with the addition of passive state improving elements, like chromium, nickel [1,2].

The hardening effect of LSA stainless steels has been widely studied for standard wrought grades, especially austenitic stainless steels. The research interest is mainly focused on the microstructure and corrosion behaviour of austenitic stainless steel treated with a laser [3-18], while ferritic [19], duplex [20] or precipitation hardening [21] grades are weakly studied. Strengthening of the surface layer to improve the resistance to erosion, corrosion and wear due to laser alloying for stainless steels can be achieved in various ways. The fusion of hard carbides particles, like Cr_3C2, SiC, TiC, WC into the steel matrix produces a hardening effect. The alloying with carbon powder or premixed powder composition (including various species) or alloying with nitrides and borides (Si_3N_4, Si_3N_4+Ti, BN, Cr-CrB_2) can also result in high strengthening effect in the surface layer [3-19]. The highest improvement of the surface layer properties regarding abrasion resistance in austenitic stainless steels can be obtained by alloying hard carbide particles such as Cr_3C_2 and Al_2O_3 ceramic particles and their mixtures with other elements, e.g. Mn-Al_2O_3 [16]. LSA of stainless steel with elemental powders (like Cr, Ni, Mo) also was studied [17,19], recently rare earth elements like Ru were also investigated [18]. Laser alloying of austenitic stainless steel with Al-Si alloy also significantly improves resistance to cavitation erosion and increases stainless steel hardness [9]. The hardening effect of LSA stainless steel in mentioned treatments is achieved due to secondary phase (carbides, nitrides, intermetallic) precipitation in the base austenitic or ferritic matrix, but such precipitates always impair corrosion resistance.

* SILESIAN UNIVERSITY OF TECHNOLOGY, FACULTY OF MECHANICAL ENGINEERING, INSTITUTE OF ENGINEERING MATERIALS AND BIOMATERIALS, 18A KONARSKIEGO STR., 44-100 GLIWICE, POLAND

Corresponding e-mail: zbigniew.brytan@polsl.pl

The LSA can introduce alloying elements to the molten metal pool in different ways, i.e. by direct powder feeding, pre-placing paste (pasting) or by filling pre-machined surface areas. For this reason, LSA is very versatile technic giving possibilities to optionally modify surface layer chemical composition, phase composition and functional properties like wear and erosion resistance. The LSA may improve surface layer properties of PM parts due to density reduction and microstructure refinement, increasing surface corrosion and mechanical properties. Already, the same surface melting with laser radiation can improve PM part surface characteristic. Moreover, the LSA of single phase PM (austenitic or ferritic) or duplex (austenite + ferrite) stainless steel with austenite of ferrite former elements can produce complex phase microstructure, composed of duplex or ferrite, austenite and martensite in the surface layer, thus improving corrosion resistance and increasing hardness [26]. In this case, LSA with adequately balanced alloying powders (pure elements, their compounds or carbides or nitrides), can establish desired steel microstructure on the surface layer. The improvement of the properties is then achieved by obtaining steel microstructure itself, free of second phase precipitates. Of course, a weaker strengthening effect can be expected in this case, but the corrosion resistance will be less degraded.

The erosion wear performance of LSA or clad coating is frequently evaluated using an air jet erosion test as described in ASTM G76 standard at different impingement angles of erodent. In the present study, solid particle erosion tests were carried out according to ASTM G76 at the impingement angle of 90° as a comparative test and expressed as relative weight loose of samples weight after erosion test. The primary purpose of such analysis was to compare LSA materials in constant conditions. Regarding a possible comparison of the results with literature data it must be noted, that present study deals with sintered materials (with some residual porosity) and are very different from wrought stainless steels.

The presented study derives and summarises some of the results described in [22-27] were PM austenitic stainless steel was laser alloyed with Cr, FeCr, the ferritic stainless steel with Ni and FeNi. Moreover, single phase stainless steels, as well as duplex stainless steel grade were LSA with SiC and Si_3N_4 powders. In the present study, the erosion resistance of such LSA sintered stainless steel was studied.

2. Methodology

2.1. The base material

Three types of sintered stainless steel were investigated. The austenitic 316L, ferritic 410L and duplex stainless steel, with the composition shown in Table 1. The austenitic and ferritic alloys were sintered form commercial powder composition of Hoeganes with the particle size of <150 μm. The third one (duplex) was produced using 410L as starting base powder mixed with addition of alloying element powders, such as Fe-Cr, Ni and Mo in the right quantity to obtain chemical composition similar to duplex stainless steel – corresponding to X2CrNiMo22-8-2 acc. to EN designation system. The detailed description of the composition preparation and resulted sintered properties were described in the paper [24]. Prepared powders were then compacted at 700 MPa in specimens of 10×10×55 mm and sintered in a vacuum with Ar backfilling at 1250-1260°C/60 min. During the sintering cycle a solution annealing at 1050°C/1h was done, and then the rapid cooling under pressure of 0.6 MPa of nitrogen was applied. The sintered stainless steel of density 7.2-7.3 g/cm^3 was obtained.

TABLE 1

The nominal chemical composition of sintered stainless steels powders used in investigations

Powder designation	Elements concentration, wt.%								
	Cr	Ni	Mo	Si	Mn	C	N	S	Fe
316LHD	16.2	12.3	2.2	0.9	0.10	0.019	0.05	0.006	bal.
410LHD	11.9	0.15	—	0.8	0.08	0.009	0.05	0.03	bal.
X2CrNiMo22-8-2	22.72	8.10	2.00	0.70	0.60	0.03	—	—	bal.

2.2. The laser surface alloying (LSA)

The laser surface alloying (LSA) was done using Rofin DL 020 high power diode laser (HPDL) laser with the following laser parameters at Ar atmosphere: radiation wavelength 808±5 nm, beam output power (continuous wave) 2300 W, beam focal length 82/32 mm, rectangular laser beam spot 1.8-6.8 mm, power density range in the laser beam plane 0.8-36.5 kW/cm^2. The laser beam power of 0.7, 1.4 and 2.1 kW and a constant scanning speed rate of 0.5 and 0.3 m/min were adopted in the studies.

The alloyed surface layers on sintered stainless steel were produced as single stringer beads; the laser beam was focused on the top of specimens. The long side of a laser beam spot was set perpendicularly to the alloying direction. The laser beam was guided along longer side (55 mm) of specimens 10×10×55 mm, the side compatible with their pressing direction.

The surface of sintered stainless steel was alloyed with different powders, like: Cr, FeCr, FeNi, SiC, Si_3N_4 using different strategies: (1) the powder injected directly into the molten metal pool by the feeder, at constant powder feed rate of 5 g/min, scanning rate 0.5 m/min; (2) the powder applied directly on the surface by filling parallel grooves (depth of 0.5 and 1.0 mm of a triangular shape – angle of 45°) machined on the sample surface, scanning rate 0.3 m/min. The sketch of different alloying powder placement strategies during LSA is shown in figure 1.

2.3. Materials characterisation

The materials microstructure was investigated by light (LOM) and scanning microscopy (SEM) with the EDS probe. The phase composition was evaluated by X-Ray diffraction (XRD) in diffraction angle 30-130° of 2θ, with the filtered Cu

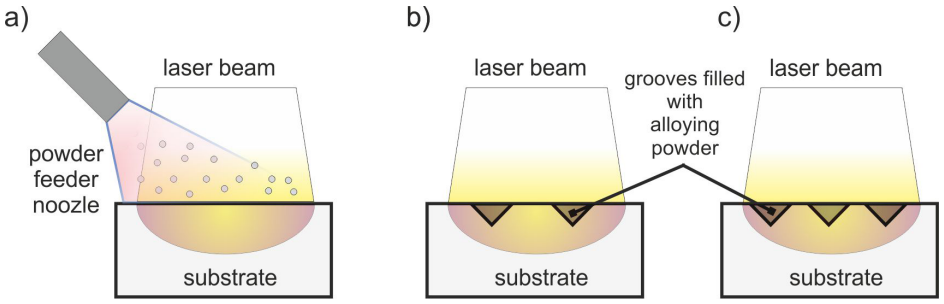

Fig. 1. Powder alloying strategies during LSA, a) powder introduced directly to the molten metal pool by the feeder, b) and c) powder pre-placed on the surface by filling the parallel grooves machined on the sample surface

lamp rays at 45 kV and heater current of 40 mA. The Vickers microhardness HV0.1 was measured on the cross-section, and depth profile of the microhardness was determined. The superficial hardness HRA of LSA samples was measured.

The erosion tests were performed to determine the erosion rate by solid particle impingement in a gas stream as described in ASTM G76 standard. The solid particles used for erosion tests were natural angular alumina sands (erodent) with a size of 80 μm. The erodent particle velocity was 70 m/s, and the feed rate of erodent was set to 2.0 g/min. The distance from the nozzle tip to the tested surface was kept at 10.0 mm. The angle of the particle impingement on the surface was 90°. The erosion test duration was 10 min. The samples were weighed (with accuracy ±0.01 g) before and after the erosion test to calculate weight loss. The solid particle erosion tests were used as a comparative method to evaluate LSA materials erosion performance, expressed as relative weight loose (‰) of samples after erosion test.

3. Results and discussion

3.1. The microstructure of LSA stainless steel

The microstructure of LSA austenitic stainless steel after, shows the different zones in a melted layer, depending on LSA strategy and laser beam power. In the case, where the alloying powder was fed directly to the molten metal pool at a constant feed rate the microstructure can be described as follows. Starting from the top surface, the first zone is enriched by alloying powder particles that protrude from the surface. Alloying powder particle (Cr, FeCr, FeNi) protrude from the surface, considerably increasing surface roughness. Particles are partially or fully melted, depending on their shape, but the bigger one remains not fully dissolved – in case of low laser beam power (i.e. 0.7 kW). The increase of laser beam power increases the next zone, the fully alloyed zone enriched in alloying element (chromium), showing the microstructure of cellular-dendritic morphology. The LSA with Cr and FeCr produce matrix saturated with chromium, that results in the duplex ($\gamma + a$) microstructure. The microstructure in this zone is composed of a ferritic matrix, where needle-shaped austenite precipitates on ferritic grains. Next, the transient zone can also be observed on the boundary of the melted zone and base material. The transient zone reveals fine dendrites, oriented in according to heat distribution direction and a sharp border of crystallisation front. With the increase of laser beam power (1.4 and 2.1 kW) majority of the melted zone is chromium enriched one of the cellular-dendritic crystals with chromium microsegregation at cell boundaries and large ferritic grains with needle-like austenite (Figs. 2,3). The change of LSA strategy, where FeCr powder fills grooves machined on surface

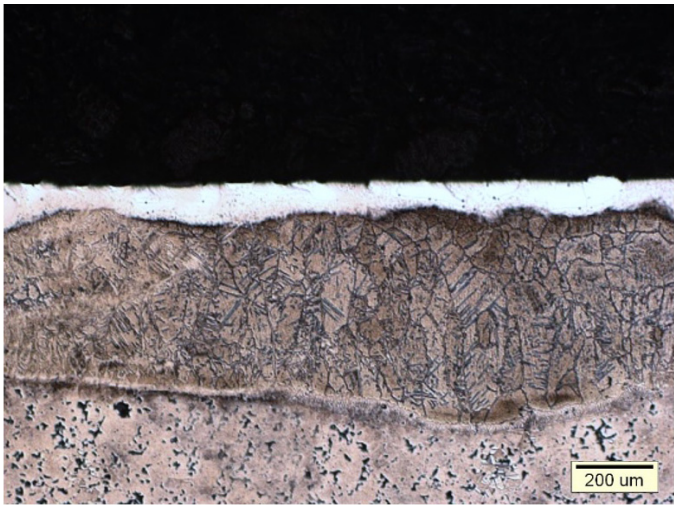

Fig. 2. Austenitic stainless steel 316L alloyed with FeCr, laser beam power 2.1 kW, powder feed directly to the molten metal pool

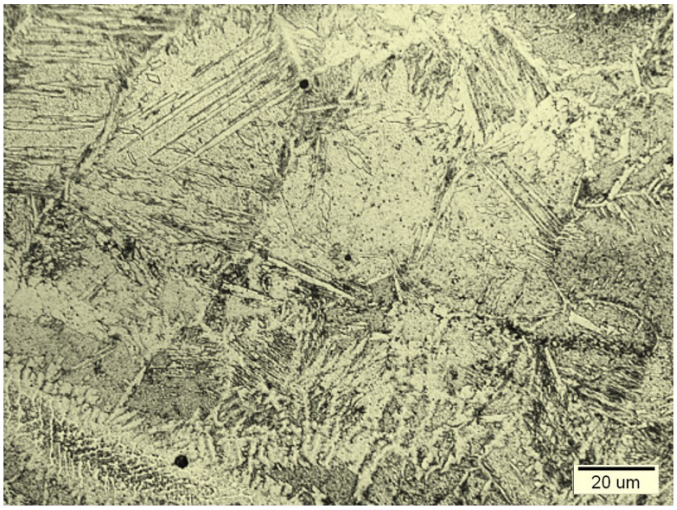

Fig. 3. Austenitic stainless steel 316L alloyed with FeCr, laser beam power 2.1 kW, powder feed directly to the molten metal pool

result in a higher dilution rate of the alloying powder. Thus, LSA of austenitic stainless steel with FeCr result in the duplex ($\gamma + a$) microstructure composed of cellular-dendritic crystals, where interdendritic and vermicular ferrite precipitates (Figs. 4,5).

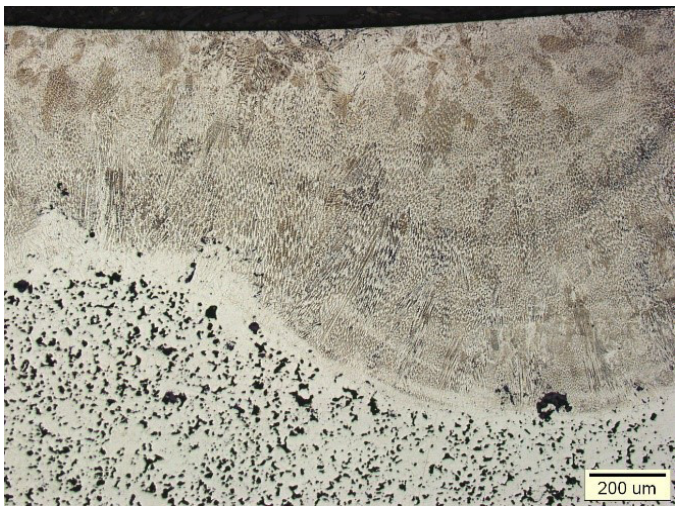

Fig. 4. Austenitic stainless steel 316L alloyed with FeCr, laser beam power 2.1 kW, powder filing 2 grooves of 1.0 mm

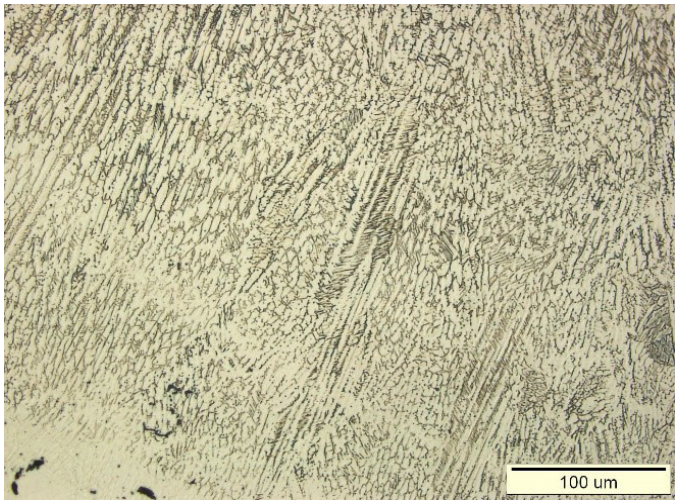

Fig. 5. Austenitic stainless steel 316L alloyed with FeCr, laser beam power 2.1 kW, powder filing 2 grooves of 1.0 mm

The scheme of LSA austenitic stainless steel microstructure and resulted in Cr and Ni content, concerning the LSA strategy of powder placement and laser beam power is shown in Fig. 6a for Cr and FeCr alloying, while in Fig. 6b for FeNi alloying. In case of LSA with 0.7 kW, the chromium content in the alloyed microstructure was hard to reliably estimate, due to high non-dissolved particle content (having the base 70%Cr/30%Fe composition). In other cases, regardless alloying parameters, chromium content was included in the range 19-30%, at 8-10%Ni and 2.5-3%Mo. Thus, corresponding to the ferritic-austenitic region in the well-known Schaeffler diagram, describing stainless steels microstructures.

When austenitic stainless steel was LSA with FeNi, the zone mentioned above was also revealed in the alloyed layer. Where

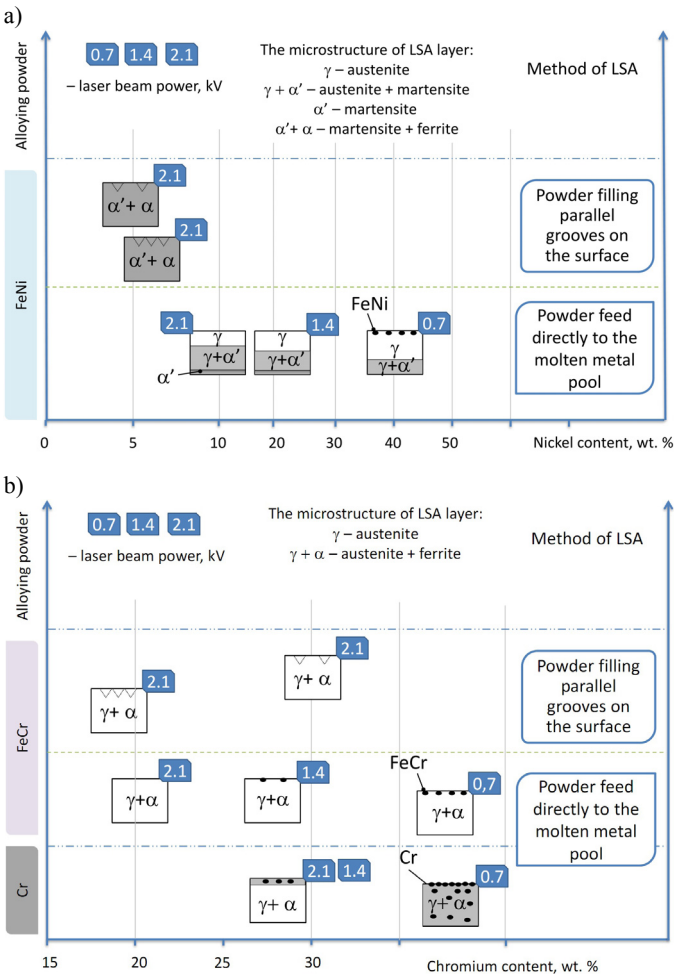

Fig. 6. The scheme of LSA stainless steel microstructure and Cr and Ni contents, in respect to LSA method and laser power beam, a) austenitic stainless steel 316L alloyed with Cr, FeCr, b) ferritic stainless steel 410L alloyed with FeNi

the alloying powder (FeNi) was fed directly to the molten metal pool at a constant feed rate, the lower dilution rate was obtained. This resulted in more complex phase formation independence to LSA parameters. In the case, where the alloying powder was fed directly into the molten metal pool at constant feed rate the microstructure can be described as follow. The microstructure alloyed zone consists of a half of the austenitic area with a cellular grain morphology that occurs on the top layer and the next region of mixed character austenitic-martensitic ($\gamma + a'$) microstructure, located at the boundary of the alloyed layer and the base metal (Fig. 7). The share of austenitic-martensitic ($\gamma + a'$) microstructure increases with applied laser beam power. The formation of a mixed-type transition zone results from the low nickel concentration in the interface boundary region (base material/alloyed layer) and the dominant martensite (a') formation mechanism from the austenitic matrix during cooling. The described transition zone with a martensitic microstructure was documented in the literature [27], where such kind of area was observed during dissimilar welding using a nickel-rich filler material, where martensite was formed in the fusion line of austenitic and ferritic stainless steel. The martensitic rich region arises as a result of balancing effects of ferrite and austenite

former elements in the equilibrium for martensitic phase. At chromium content 9-14% in the base material, the falling nickel concentration contributes to austenite stability reduction along with the increase of laser beam power and leads to the formation of austenitic, mixed austenitic-martensitic and martensitic structures (Fig. 6b). In the top surface of the alloyed layer, insoluble FeNi powder particles were observed only for the lowest laser beam power 0.7 kW.

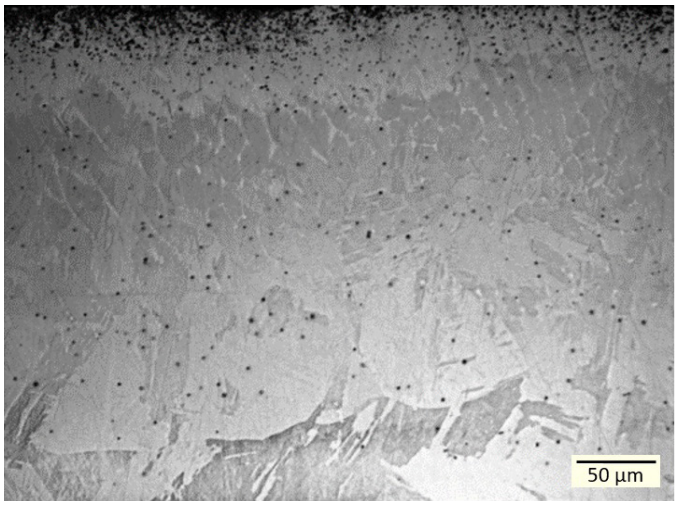

Fig. 7. Ferritic stainless steel 410L alloyed with FeNi, laser beam power 0.7 kW, powder feed directly to the molten metal pool

The LSA of ferritic stainless steel with FeNi powder, dispensed by the feeder, makes it possible to obtain in the alloyed layer from approx. 40%, through 20% to 10% of nickel, respectively at a laser beam power of 0.7 kW, 1.4 kW and 2.1 kW (Fig. 6b). An inverse relationship between applied laser beam power and the nickel concentration was found, that result from accelerated melting and mixing of the alloying material at higher laser beam power. The second LSA strategy, where FeNi powder was filled to grooves machined on the sample surface result in even more dilution of alloying powder. That gives nickel concentration at 5-7% and predominantly martensitic-ferritic (*a'* + *a*) microstructure (Fig. 8).

The LSA of tree stainless steel substrates (austenitic, ferritic and duplex) with SIC and SI_3N_4 powders was performed by filling the grooves machined on samples surface. Such a strategy was selected to obtain the highest dilution ratio of alloyed powder. The main scope was to dissolve the alloying powder completely during LSA, and form microstructures saturated possibly high in either carbon or nitrogen, that are strong austenite former elements.

During LSA with SiC, the dissolution of SiC powder take place and leads to precipitations of silicon-rich phases like Fe_3Si, Cr_5Si_3, Fe_2Si, and complex carbides C-Fe-Si, M_7C_3 type, depending on the dilution rate in the alloyed layer. The microstructure of austenitic stainless steels alloyed with SiC reveals primary dendrites of the austenite phase and interdendritic lamellar eutectics of austenite and carbides M_7C_3 (Fig. 9). For more diluted alloying powder option (3 grooves 0.5 mm)

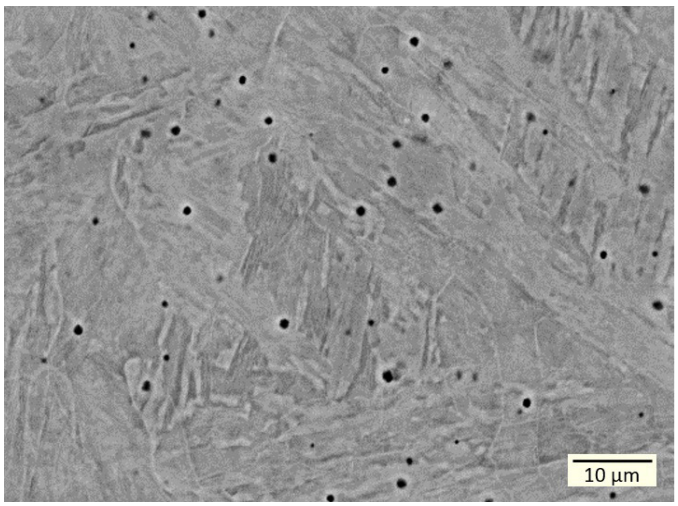

Fig. 8. Ferritic stainless steel 410L alloyed with FeNi, laser beam power 2.1 kW, powder filling 3 grooves of 0.5 mm (SEM)

the interdendritic regions are narrow, and lamellar eutectic of austenite and carbides weakly visible (Fig. 10). For less diluted powder (2 grooves of 1.0 mm) in the microstructure of alloyed layer shows dendrites having shorter arms and coarser interdendritic regions with lamellar structures (Fig. 11). EDS analysis confirmed, that austenitic dendrites reveal increased Ni and Fe content, while the eutectic zones are enriched in C, Cr, Si and Mo. Similarly, in the microstructure of ferritic stainless steel LSA with SiC formation of martensitic laths was observed in primary austenitic dendrites, while in the interdendritic region more developed lamellar structures (Fig. 12). The LSA duplex alloy revealed the same complex microstructure of a fine dendritic character with the interdendritic lamellar eutectic. The top of alloyed layer was more inhomogeneous regarding formed microstructure and observed phases. The silicon distribution in the all bulk alloyed layer was stable, showing approx. 4-7% depending on process conditions.

During LSA with Si_3N_4, the stainless steels microstructure become enriched in silicon and nitrogen due to decomposition

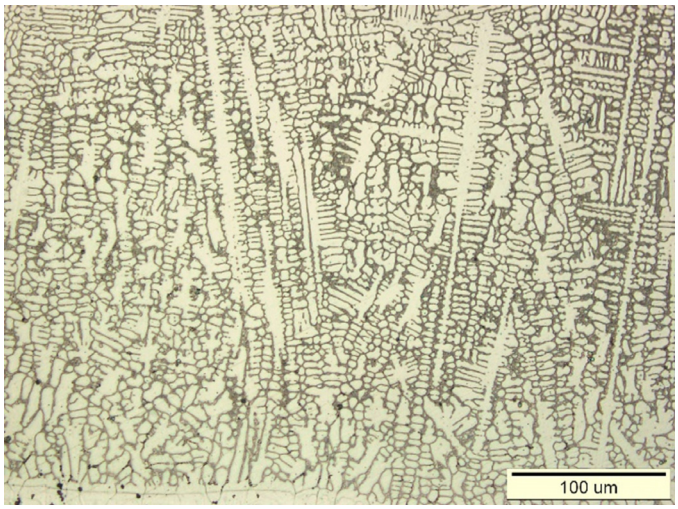

Fig. 9. Austenitic stainless steel 316L alloyed with SiC, laser beam power 2.1 kW, powder filling 2 grooves of 1.0 mm

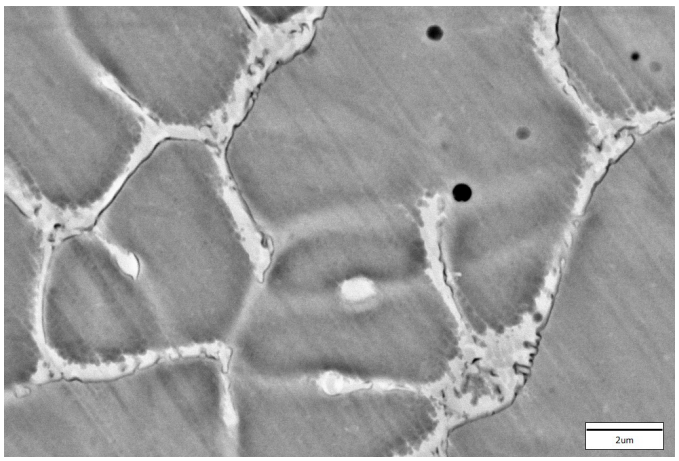

Fig. 10. Austenitic stainless steel 316L alloyed with SiC, laser beam power 2.1 kW, powder filling 3 grooves of 0.5 mm, (SEM)

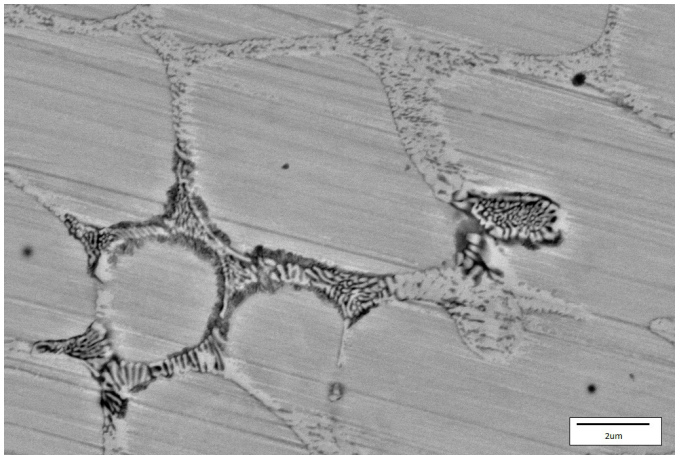

Fig. 11. Austenitic stainless steel 316L alloyed with SiC, laser beam power 2.1 kW, powder filling 3 grooves of 1.0 mm, (SEM)

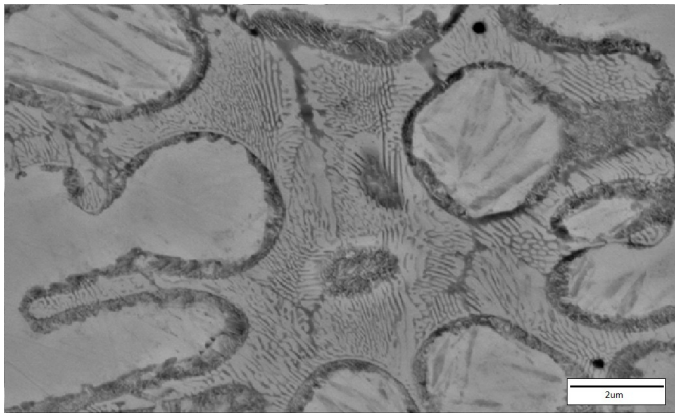

Fig. 12. Ferritic stainless steel 410L alloyed with SiC, laser beam power 2.1 kW, powder filling 3 grooves of 1.0 mm, (SEM)

of Si_3N_4 to Si and N that stabilise austenitic phase. The powder particles were fully dissolved during laser processing, also in the top surface layer zone. The austenitic stainless steel LSA with Si_3N_4 was composed of cellular-dendritic regular grains with visible alloying elements segregation on the grain boundaries. The strong austenite stabilisation effect of N was observed in ferritic stainless steel, where steel microstructure become complex ferritic-martensitic (and some austenite). On the primary massive ferritic grains precipitated austenite, that transformed to lamellar martensite, along with the grains borders and towards ferritic grains and inside ferritic grains (Fig. 13).

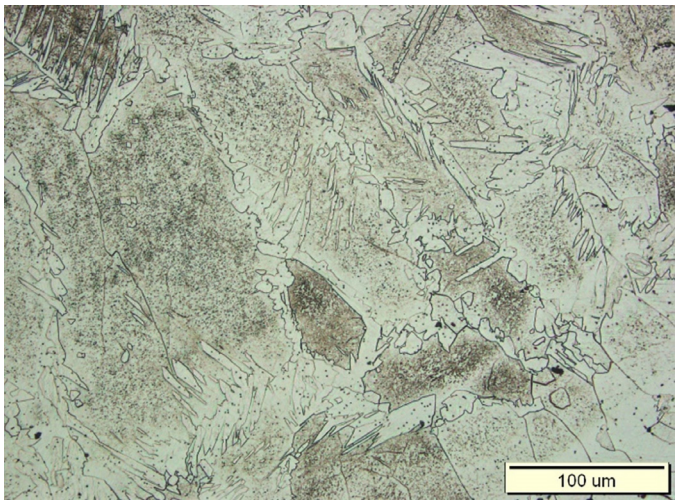

Fig. 13. Ferritic stainless steel 410L alloyed with Si_3N_4, laser beam power 2.1 kW, powder filling 2 grooves of 1.0 mm

LSA duplex alloy shows very fine austenite+ferrite ($\gamma + a$) microstructure, with a high content of fine acicular austenite precipitated along primary ferritic grain boundaries and extensively inside ferritic grains (Fig. 14). The rapid solidification of the LSA process, leading to ferrite content increase was balanced by austenite stabilising effect of nitrogen decomposed from Si_3N_4, thus resulted duplex microstructure is well balanced in both phases. Medium silicon content for all three kinds of LSA stainless steel was 2-4% depending on process conditions.

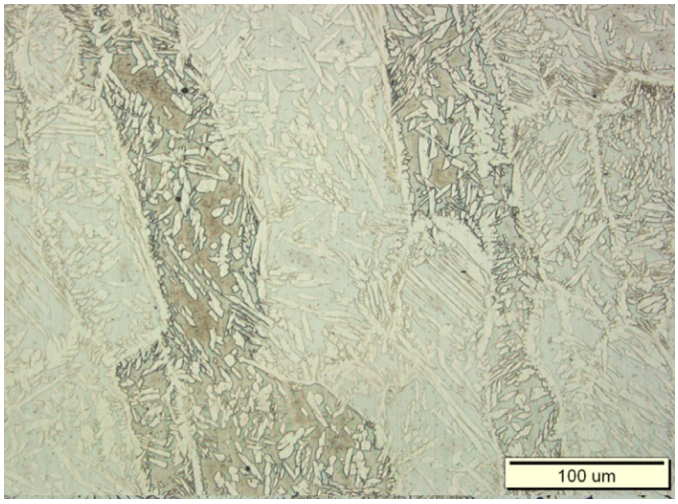

Fig. 14. Duplex stainless steel alloyed with Si_3N_4, laser beam power 2.1 kW, powder filling 2 grooves of 1.0 mm

Tables 2 and 3 summarised LSA process parameters and resulted in main microstructural phases, confirmed by XRD phase analysis.

TABLE 2

Laser parameters, meld depth and microstructure characteristics of specimens laser surface-alloyed with Cr, FeCr and FeNi

Specimen / alloying powder		Method of LSA		Laser power P (kW)	Melt depth D (mm)	Main phases (XRD and SEM analysis)
316L	Cr	Powder feed directly to the molten metal pool, scanning rate 0.5 m/min		0.7	0.14	Fe γ, Fe a
				1.4	0.40	
				2.1	0.88	
	FeCr			0.7	0.17	
				1.4	0.29	
				2.1	0.86	
410L	FeNi			0.7	0.10	Fe γ, Fe a (a')
				1.4	0.21	Fe γ, Fe a (a')
				2.1	0.45	Fe γ, Fe a (a') + a'
316L	FeCr	Powder filling parallel grooves on the surface, scanning rate 0.3 m/min	2 grooves 1.0 mm	2.1	1.23	Fe γ, Fe a
			3 grooves 0.5 mm	2.1	1.13	
410L	FeNi		2 grooves 1.0 mm	2.1	0.83	Fe a + a'
			3 grooves 0.5 mm	2.1	0.56	

TABLE 3

Laser parameters, meld depth and microstructure characteristics of specimens laser surface-alloyed with SiC and Si3N4

Specimen / alloying powder		Method of LSA	Quantity / grooves depth machined on the surface (mm)	Melt depth D (mm)	Main phases (XRD and SEM analysis)
316L	SiC	filling parallel grooves on the surface, scanning rate 0.3 m/min, laser beam power 2.1 kW	2 / 1.0 mm	1.21	Fe γ, Fe_3Si, Cr_5Si_3, Fe_2Si, C-Fe-Si, M_7C_3
			3 / 0.5 mm	0.93	
410L			3 / 1.0 mm	1.04	Fe γ, Fe a (a'), Fe_3Si, Fe_2Si, C-Fe-Si and M_7C_3
			3 / 0.5 mm	0.64	
Duplex			3 / 1.0 mm	1.16	Fe γ + Fe a (matrix), FeSi, Fe_3Si, C-Fe-Si, M_7C_3
			3 / 0.5 mm	1.05	
316L	Si_3N_4		2 / 1.0 mm	1.31	Fe γ
			3 / 0.5 mm	1.02	
410L			3 / 1.0 mm	0.97	Fe a (a')
			3 / 0.5 mm	0.61	
Duplex			3 / 1.0 mm	1.27	Fe γ + Fe a
			3 / 0.5 mm	1.34	

3.2. The mechanical properties of LSA stainless steel

The base material, in as-sintered condition, shows the hardness of 35±2 HRA for austenitic and ferritic stainless steel, while duplex alloy is slightly harder, 43±2 HRA. The superficial hardness HRA of LSA stainless steels at different alloying process parameters is shown in Figs. 15 and 16. LSA increase surface hardness proportionally to applied laser beam power, where higher laser beam energy facilitates dissolution of alloying powder, and increase the saturation of molten metal pool by alloying elements. Thus, complex microstructures and secondary phases can precipitate, having a higher hardness. Besides that, the LSA primarily reduce initial material porosity, characteristic for PM parts and cause densification of melted and solidified material, together with subsequent alloying be additional powders. The most substantial effect in hardness increase can be observed for 2.1 kW laser treated samples. Regarding alloying powders, they hardening effect is the strongest for SiC powder (61-79HRA), due to hard silicides and carbides precipitation, as described in the previous section. Next, LSA with FeNi (43-68HRA) acts strongly on the microstructure hardening, due to precipitation and formation of complex microstructures with martensite presence. Other alloying powders (Cr, FeCr, Si_3N_4) during LSA cause formation of the ferritic or austenitic microstructure to form duplex microstructure, also giving an increase of hardness in respect to the base single-phase material microstructure.

The more detailed look, on the microhardness (HV0.1) distribution on the cross-section of LSA stainless steel, for example with Cr and FeCr, reveal higher microhardness in the top layer, where no dissolved powder particles are present (Fig. 17). The central alloyed zone shows uniform microhardness profile, till the end of melting, where hardness sharply decrease to values characteristic for a base material (c.a. 100HV0.1). Depending on laser beam power, so melting intensity, the most uniform microhardness profile of high melting dept is obtained for 2.1 kW. The lower laser power (0.7, 1.4 kW) produce lower melting dept, but of higher microhardness values (Fig. 17b). When increasing dilution rate of LSA treatment, by filling powder into grooves

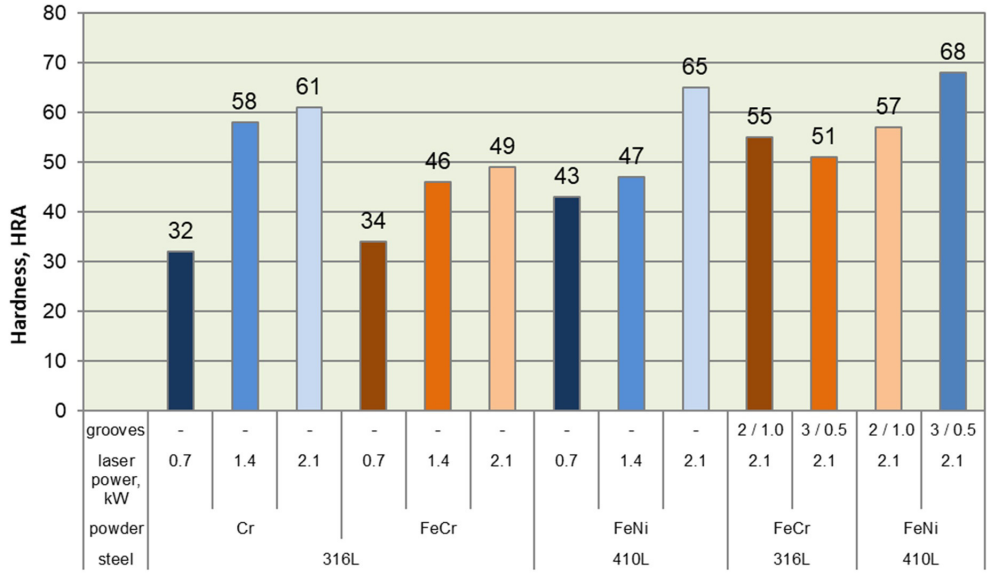

Fig. 15. The superficial hardness stainless steels LSA with a) Cr, FeCr and FeNi powders feed directly to the molten metal pool and alloyed with different laser beam powers (0.7-2.1 kW), scanning rate 0.5 m/min, b) FeCr and FeNi powders filled into grooves machined on the surface, laser beam power 2.1 kW, scanning rate 0.3 m/min

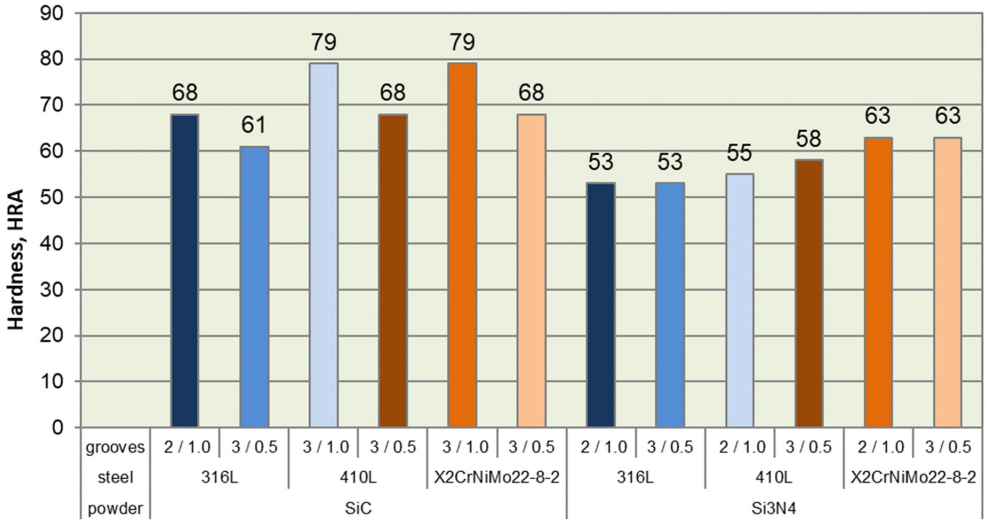

Fig. 16. The superficial hardness of austenitic (316L), ferritic (410L) and duplex (X2CrNiMo22-8-2) stainless steels LSA with a) SiC powder and b) Si_3N_4 powder filled into grooves machined on the surface, laser beam power 2.1 kW, scanning rate 0.3 m/min

machined on the surface, the microhardness profile is more constant and uniform with lower maximum hardness values (Fig. 17c) Similarly changing the number of depth of grooves with powder (Fig. 18). The described relation was valid for all teste LSA parameters.

3.2. The erosion test of LSA stainless steel

The erosion tests of LSA stainless steels with different alloying strategies shows a relative weight loss in the wide range from 0.08 to 0.7‰ (Figs. 19, 20).

In the case of non-laser treated stainless steels in as sintered conditions, the lowest relative weight loss was found for 410L ferritic stainless steel, which was 0.09‰, while for austenitic 316L and duplex X2CrNiMo22-8-2 steel was 0.10 and 0.11‰ respectively. The sintered stainless steels base material in as sintered conditions, without laser surface treatment, show a lower relative weight loss of material during the erosion test compared to most of the LSA samples. This phenomenon can be explained by the low hardness of sintered stainless steels and high plasticity and immune porosity of the sintered material. The porosity, during erosion test, undergoes plastic deformation by erodent impingement and causes local densification of material in the crater region, thus not causing substantial weight loss of material. The erosion resistance of LSA stainless steel surface was evaluated at the erosive angle of 90°, for which the material is consumed by spalling-out of micro-sized hardened material particles, exhibiting brittle-type behaviour, characteristic for brittle materials.

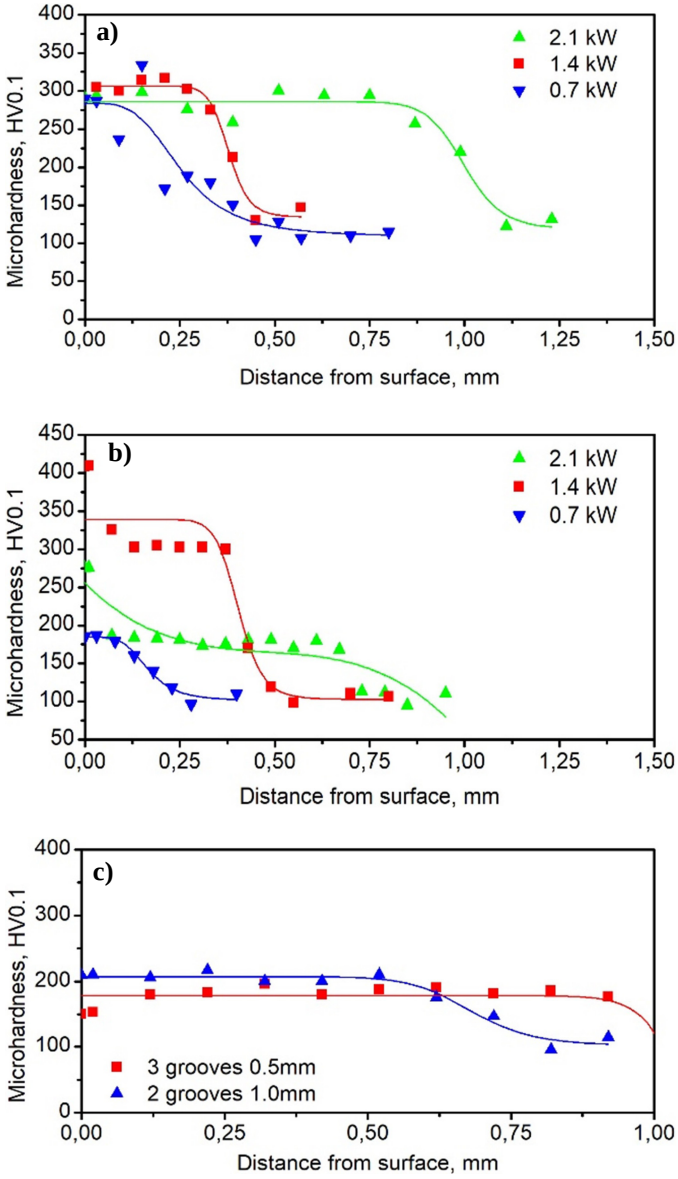

Fig. 17. Microhardness HV0.1 profile of austenitic 316L stainless steel LSA with a) Cr, b) FeCr powder feed directly to the molten metal pool at different laser beam power (0.7-2.1 kW) and c) FeCr powder filling grooves on the sample surface at constant laser beam power 2.1 kW

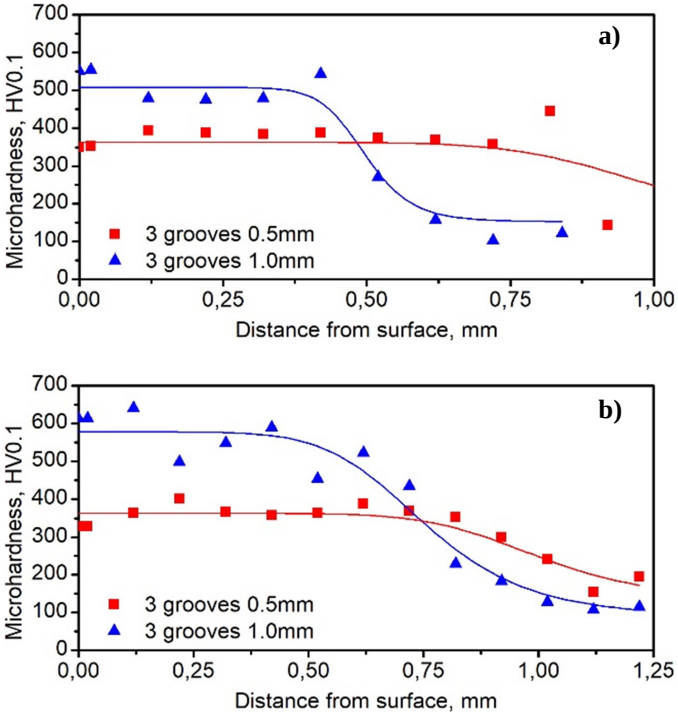

Fig. 18. Microhardness HV0,1 profile of stainless steel LSA with SiC, a) ferritic 410L stainless steel, b) duplex stainless steel X2CrNiMo22-8-2, laser beam power 2.1 kW, powder filling grooves on the sample surface

The results of erosion tests depend on the amount of alloying material introduced to the liquid metal pool during alloying. Basing on relative weight loss after erosion test was found that the increase of the laser power during alloying of the austenitic steel 316L with Cr and FeCr powders introduced to the liquid metal pool by the feeder reduces the erosion rate of the surface layer. A positive effect of no-fully dissolved powder particles present in the top area of a remelted layer can be related to such effect. In the case of ferritic stainless steel 410L alloyed with FeNi powder also introduced to the alloying zone by the feeder, the lowest relative weight loss of 0.08‰ was obtained for alloying with a 2.1 kW of laser beam power (Fig. 19, on the left). The results of erosion test of LSA with the powder feeding strategy are strongly related to applied laser beam power. In general, the use of a maximum laser beam power of 2.1 kW increases the resistance to erosion of the alloyed surface of studied stainless steels. For samples with machined grooves filled with alloying powder (FeCr, FeNi) and then remelted, it was found that the highest resistance to erosion wear shows alloyed layers, where more material was introduced to the melting zone – samples with two grooves of 1.0 mm (Fig. 19, on the right).

Figure 20 presents the relative weight loss after erosion test for austenitic 316L, ferritic 410L and duplex X2CrNiMo22-8-2 stainless steels, LSA with SiC and Si_3N_4 powders, where the strategy of LSA based on powder filled grooves machined on the sample surface was introduced. The SiC alloyed surfaces show the lowest weight loss for a surface with three grooves a depth of 0.5 mm. In this, case less alloying material work better regarding weight loose during erosion. The SiC LSA ferritic stainless steel with three grooves of 1.0 mm shows increases of relative weight loss of the samples to 0.7‰, which is the maximum value compared to the other tested conditions. In this case, numerous cracks in the alloyed layer and porosities were observed in the area of erosion crater. Such low resistance to the erosive wear results from high saturation of the surface layer in carbon, which leads to many precipitates of hard carbides and silicides which break brittle under the influence of erodent and accelerate the weight loss of the surface in an expedited manner. As can be seen, the alloyed layer microstructure plays a crucial role during erodent impingement. The harder and brittle microstructure matrix the faster braking and spalling of steel matrix.

In the case of LSA with Si_3N_4 powder (Fig. 20), the relationship between LSA strategy and surface preparation by machining grooves and the resistance to erosive wear was not

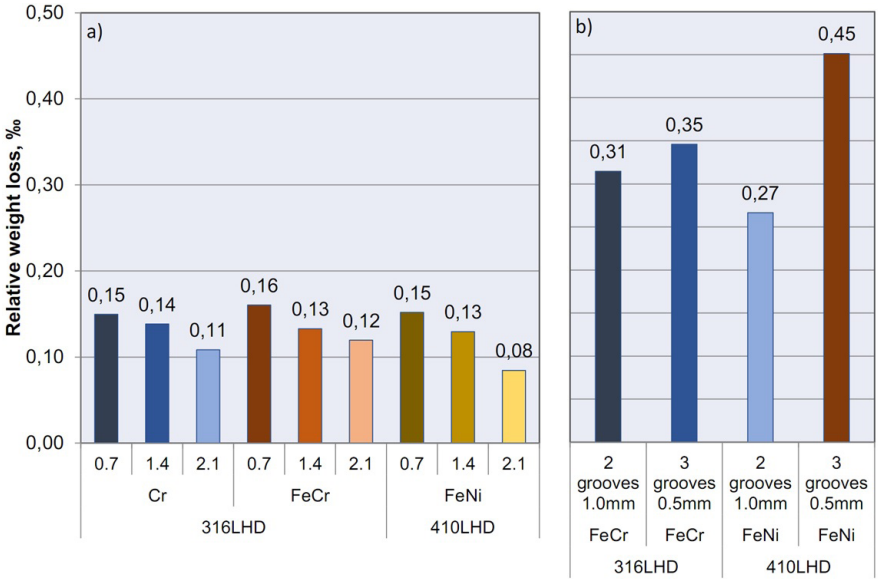

Fig. 19. The relative weight loss in erosion test of stainless steels LSA with Cr, FeCr and FeNi powders feed directly to the molten metal pool and alloyed with different laser beam power (0.7-2.1 kW), scanning rate 0.5 m/min (on the left) and LSA with FeCr and FeNi powders filled into grooves machined on the surface, laser beam power 2.1 kW, scanning rate 0.3 m/min (on the right)

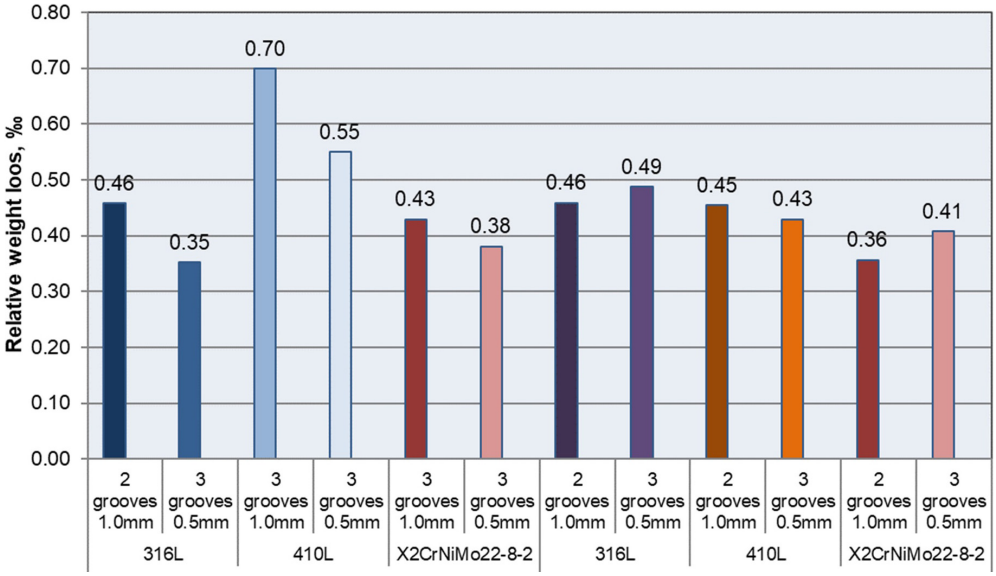

Fig. 20. The relative weight loss in erosion test for stainless steels LSA with SiC powder and Si_3N_4 powder filled into grooves machined on the surface, laser beam power 2.1 kW, scanning rate 0.3 m/min

clearly disclosed. The Si_3N_4 decomposition to N and Si during LSA lead to the preferential formation of the austenitic phase, that is more plastic and softer than ferrite. The erosion resistance despite alloying powder dilution rate was more the same for a given substrate material. The LSA austenitic alloy, which is softer performed better than harder ferritic and duplex stainless steel. For austenitic and ferritic stainless steel LSA with Si_3N_4 powder, filled into three grooves with a depth of 0.5 mm in areas of erosion crater various porosities were observed, which testify an intensive spalling of micro-sized material volume because of surface fatigue during the test. The lowest relative weight loss of 0.36‰ was registered for duplex steel grade where the powder filled two grooves of 1.0 mm.

4. Conclusions

The LSA with ferrite and austenite former elements, like Cr, FeCr, FeNi contribute to microstructural changes to form a complex microstructure of LSA stainless steel. Thus, the duplex microstructure can be obtained on the austenitic substrate by LSA with Cr and FeCr. The complex microstructure of austenite, ferrite and martensite were revealed for LSA ferritic stainless steel. The LSA with Si_3N_4 also strongly increased austenite content in the ferritic and duplex stainless steel. The LSA with SiC revealed the highest potential of hardness increase for studied alloys.

Erosion resistance of LSA stainless steels is not only related to superficial hardness or microhardness profile but also strictly

depends on the base material properties (microstructure). The softer and ductile austenitic stainless steel resist better than harder ferritic and duplex stainless steel material at studied erodent impingement angle of 90°. The erosion wear is lower for Cr, FeCr, FeNi laser alloying, where powders were dissolved in the steel microstructure, and hard phases were not precipitated – introducing powder directly to the molten metal pool. Precipitations of hard phases (carbides, silicides, martensite formation) reduce erosion resistance of SiC alloyed stainless steel. LSA with Si_3N_4 works better – lack of precipitates and creation of a soft austenitic microstructure.

The erosion resistance of tested stainless steels deteriorates depending on related LSA treatment conditions comparing to as-sintered state. Sintered stainless steels without laser alloying undergo local compaction during perpendicular striking of erodent to the surface, showing low weight loss in erosion test and ductile erosion mode as for wrought austenitic stainless steel, i.e. AISI 304 [28].

The erosion wear at the impingement angle of 90° of the erodent is high for hard and therefore brittle surface layers obtained as a result of alloying by hard particles (SiC, Si_3N_4). On this basis, it can be expected that at lower incidence angles close to 30° and 45° their erosion wear can be lower. While for ductile materials, less hardened by LSA in this case, the higher erosive wear can be expected at more moderate incidence angles.

Acknowledgements

This publication was financed by the Ministry of Science and Higher education of Poland as the statutory financial grant of the Faculty of Mechanical Engineering SUT.

REFERENCES

[1] L.A. Dobrzanski, T. Tanski, A.D. Dobrzanska-Danikiewicz, E. Jonda, M. Bonek, A. Drygala, Laser Surface Engineering: Processes And Applications, Edited by: Lawrence J.; Waugh, DG, Book Series: Woodhead Publishing Series in Electronic and Optical Materials **65**, 3 (2015).

[2] J.M. Dutta, I. Manna, Laser processing of materials, Sadhana--Acad. P. Eng. S. **28**, Parts 3, 495, June/August 2003.

[3] J.C. Betts, J. Mater. Process. Tech. **209**, 5229 (2009).

[4] F. Laroudie, C. Tassin, M. Pons, J. Mater. Sci. **30**, (1995) 3652.

[5] D. Zhang, X. Zhang, Surface Coat. Tech. **190**, 212 (2005).

[6] J.M. Dutta, I. Manna, Mater. Sci. Eng. A **267**, 50 (1999).

[7] C.T. Kwok , F.T. Cheng, H.C. Man, Mater. Sci. Eng. A **290**, 55 (2000).

[8] C.T. Kwok, H.C. Man, F.T. Cheng, Surface Coat. Tech. **99**, 295 (1998).

[9] S. Zherebtsov, K. Meakawa, T. Hayashi, M. Futakawa, JSME Int. J. Series A, **48**, 4, 292 (2005).

[10] M.U. Kamachi, K.R. Ningshen, S. Ganesh, P. Nath, A.K. Khatak, HS. Baldevraj, Mat. Sci. Tech. **22**, 10, 1185 (2006).

[11] Q.Y. Pan, W.D. Huang, R.G. Song, Y.H Zhou, G.L. Zhang, Surf. and Coat. Technol. **102**, 245 (1998).

[12] C. Carboni, P. Peyre, G. Beranger, C. Lemaitre, J. Mater. Sci. **37**, 3715 (2002).

[13] A. Viswanathana, D. Sastikumar P. Rajarajan, Harish Kumar, A.K. Nath, Opt. Laser Technol. **39**, 1504 (2007).

[14] A. Conde, I. Garcia, J. Damborenea, Corrosion Sci. **43**, 817 (2001).

[15] J. Ion, Laser Processing of Engineering Materials: Principles, Procedure and Industrial Application, Butterworth-Heinemann, 2005.

[16] P. Li, G.F. Sun, W. Zhang, W.X. Liuw, Y.K. Zhang, M.K. Zhang, The Chinese Journal of Nonferrous Metals **22** (8), 2253 (2012).

[17] D. Zhang, X. Zhang, Surf. Coat. Tech. **190**, 212-217 (2005).

[18] N.N. Tshilwane, J.W. van der Merwe, Surf. Coat. Tech. **347**, 414 (2018).

[19] X. Tong, M.J. Dai, Z.H. Zhang, Appl. Surf. Sci. **271**, 15, 373 (2013).

[20] P.H. Lailatul, M.A. Maleque, Proc. Eng. **184**, 737 (2017).

[21] J. Yao, L. Wang, Q. Zhang, F. Kong, Ch. Lou, Z. Chen, Opt. Laser Technol. **40**, 838 (2008)

[22] Z. Brytan, M. Bonek, L.A. Dobrzański, W. Pakieła, Adv. Mat. Res. **291-294**, 1425 (2011).

[23] Z. Brytan, L.A. Dobrzański, W. Pakieła, J. Achiev. Mater. Manuf. Eng. **47**, 1, 42 (2011)

[24] Z. Brytan, L.A. Dobrzański W. Pakieła, Arch. Mater. Sci. Eng. **50**, 1, 43. (2011).

[25] Z. Brytan, M. Bonek, L.A. Dobrzański, J. Achiev. Mater. Manuf. Eng. **40**, 1, 70 (2010).

[26] Z. Brytan, Proceedings of Asia International Conference on Tribology 2018, September 2018, red. Mohd Fadzli Bin Abdollah, Malaysian Tribology Society, 376.

[27] J.N. Dupont, C.S. Kusko, Technical Note: Martensite Formation in Austenitic/Ferritic Dissimilar Alloy Welds, 51, Weld J, February 2007.

[28] M. Patel, D. Patel, S. Sekar, P.B. Tailor, P.V. Ramana, Proc. Tech. **23**, 288 (2016).